Available online at www.sciencedirect.com

ScienceDirect

Energy Procedia 140 (2017) 36–47

Energy Procedia

www.elsevier.com/locate/procedia

AiCARR 50th International Congress; Beyond NZEB Buildings, 10-11 May 2017, Matera, Italy

# Analytical modelling of Breathing Walls: experimental verification by means of the Dual Air Vented Thermal Box lab facility

Andrea Alongi[a], Adriana Angelotti[a,*], Livio Mazzarella[a]

[a]*Politecnico di Milano, Dipartimento di Energia, via Lambruschini 4, Milano 20156, Italy*

**Abstract**

Breathing Walls are air permeable envelope components based on porous materials. In *contra-flux* operation air flows opposite to conductive flux, while in *pro-flux* they have the same direction. The Breathing Wall behaves either as a ventilation heat exchanger or as an active insulation.
In literature an analytical model describing steady state heat transfer across a Breathing Wall can be found. Since it lacks an exhaustive experimental validation, a facility developed at the Energy Department of Politecnico of Milano was used to investigate the thermo-physical behavior of a no-fines concrete based Breathing Wall in steady state Dirichlet conditions and contra-flux operation.


Peer-review under responsibility of the scientific committee of the AiCARR 50th International Congress; Beyond NZEB Buildings.

*Keywords:* dynamic insulation; breathing wall; porous materials; experimental validation; laboratory facility.

## 1. Introduction

Dynamic Insulation technology, also known as Breathing Wall, has been object of study since the early Nineties [1], as a promising approach for energy needs reduction in buildings, and its operating principles have been discussed in earlier works [2] and very recent ones [3].

* Corresponding author. Tel.: +39-02-2399-5183; fax: +39-02-2399-3913.
*E-mail address:* adriana.angelotti@polimi.it

1876-6102 
Peer-review under responsibility of the scientific committee of the AiCARR 50th International Congress; Beyond NZEB Buildings
10.1016/j.egypro.2017.11.121

**Nomenclature**

| | |
|---|---|
| $c$, $c_p$ | specific heat, *J/(kg·K)* |
| $L$ | sample thickness, *m* |
| $t$ | time, *s* |
| $T$ | temperature, *°C* |
| $u$ | airflow velocity, *m/s* |
| $x$ | coordinate along the sample thickness, *cm* |
| *Greek symbols* | |
| $\varepsilon$ | porosity, ND |
| $\phi$ | diameter, *mm* |
| $\lambda$ | thermal conductivity, *W/(m·K)* |
| $\rho$ | density, *kg/m³* |
| *Subscripts* | |
| $f$ | quantity referred to the fluid phase |
| $s$ | quantity referred to the solid phase |
| $w$ | quantity referred to the overall porous medium |

Its thermo-physical behavior has been theoretically investigated mainly in steady state conditions [4],[5], providing analytical equations for the temperature distribution in the wall both for Dirichlet and Neumann boundary condition. These equations show a deviation from the linear trend expected in a traditional wall and identify two working conditions with corresponding temperature distributions: contra-flux (airflow and heat flux have opposite directions) and pro-flux (airflow and heat flux have the same direction).

Even though the physical model has been accepted by the scientific community, the few past experimental works present data related to surface temperatures and heat fluxes in contra-flux operating mode [5]-[7], while the overall temperature distribution inside the Breathing Wall section has never been experimentally investigated and validated.

In this study, the thermo-physical behavior of a Breathing Wall in contra-flux operating mode in steady state conditions is experimentally investigated by means of the Dual Air Vented Thermal Box (DAVTB) apparatus. The DAVTB apparatus, preliminary discussed in [8], is presented, along with the thermo-physical and geometrical characterization of a no-fines concrete sample, which was object of experimental investigation. Data about the temperature distribution inside the sample were collected and compared to the corresponding physical model [4], in order to assess its reliability.

## 2. The physical model

Considering an isotropic porous medium where local thermal equilibrium between the fluid and the solid phase can be assumed, and taking averages over an elemental volume of the medium, the energy equation that takes into account both conduction and advection is given by [9]:

$$\left(\rho c\right)_w \frac{\partial T}{\partial t} + \left(\rho c_p\right)_f \nabla \cdot \left(\mathrm{u}T\right) = \nabla \cdot \lambda_w \nabla T \tag{1}$$

where $T$ and $u$ are respectively the temperature distribution and the fluid velocity field across the wall (i.e. Darcy velocity), $\rho$, $c$ and $\lambda$ are respectively the density, the specific heat (at constant pressure when related to a gas) and the thermal conductivity, referred to the overall porous material ($w$ subscript) or the air only ($f$ subscript). For steady state conditions in a one-dimensional homogeneous porous medium Equation (1) becomes [4]:

$$\lambda_w \frac{d^2T}{dx^2} - u\left(\rho c_p\right)_f \frac{dT}{dx} = 0 \tag{2}$$

As far as boundary conditions for Equation (2) are concerned, in [4] surface temperature are assumed as known (Dirichlet boundary conditions), while in [5] operative temperatures are known (Neumann boundary conditions). Since adopting Neumann boundary conditions requires knowing the convective-radiative heat transfer coefficient on both surfaces, whose determination is be-yond the scope of the present study, we report here the analytical solution of the temperature distribution in a single layer domain under Dirichlet boundary conditions.

Therefore, by introducing the parameter *A* as:

$$A = \frac{u\left(\rho c_p\right)_f}{\lambda_w} \tag{3}$$

we obtain

$$\frac{T(x) - T_0}{T_L - T_0} = \frac{e^{Ax} - 1}{e^{AL} - 1} \tag{4}$$

where $T_0$ and $T_L$ represent the superficial temperatures (boundary conditions at $x=0$ and $x=L$), L is the overall wall thickness, and the spatial coordinate $x$ goes from outdoor to indoor. The scope of the present study was to validate experimentally Equation (4).

## 3. Materials and methods

In this section the Breathing Wall sample construction used in the experimental test is firstly presented and characterized. Secondly, the Dual Air Vented Thermal Box facility as well as its control and data acquisition system are presented.

### *3.1. The concrete sample*

In this work, a specimen of no-fines concrete was studied. This material, also known as Air Permeable Concrete (APC) or pervious concrete, is a cement-based mixture, produced without small diameter aggregates. This leads to a highly porous hardened solid matrix, with highly interconnected pores, which was already studied in [10]. Taking into account its thermo-physical properties, it can be considered a suitable choice for dynamic insulation technology, in order to develop a stratified technical solution optimized for Mediterranean climate conditions in NZEB applications.

A 1 $m^2$ sample wall was built, with a thickness of 15 cm (Fig. 1), using the mix-design reported in Table I. Because of its considerable weight, the sample was divided into 9 elements, 5 of which have 9 thermocouples embedded, equally spaced along the cross-section, and 2 thermocouples attached to the exposed surfaces. This allows to monitor the temperature distribution in the blocks during every laboratory test. In the work presented in this paper, we focused our analysis on the central block, which it is far enough from the perimeter to allow disregarding any edge effects. At this point, it is important to notice that the casting procedure was carefully performed, in order to avoid any damage to the embedded thermocouple junctions. However, the overall process may have affected the probes position: this aspect will be considered in the discussion of the experimental results.

Fig. 1. The no-fines concrete sample.

Table 1. Mix-design used to produce the no-fines concrete blocks.

| | |
|---|---|
| cement powder | Portland cement CEM II-A-L/42.5 |
| aggregate | Zandobbio limestone<br>• 60% large gravel ($\phi$ = 9÷12 mm)<br>• 40% medium gravel ($\phi$ = 6÷9 mm) |
| water/cement ratio (w/c) | 0.39 |
| aggregate/cement ratio (agg/c) | 7.03 |

Before starting the experimental investigation of the overall wall in the DAVTB, the material under discussion was characterized in terms of thermo-physical properties and structure geometry.

First of all, its thermal conductivity was assessed according to some simplifying assumptions, generally adopted in the literature dealing with dynamic insulation. By disregarding the solid-fluid interaction at microscopic level and by assuming that heat conduction in the solid and fluid phases occurs in parallel [9],[11], the thermal conductivity of the porous medium is equal to the volume average of the solid and fluid parts as in Equation (5):

$$\lambda_w = \varepsilon \cdot \lambda_f + (1-\varepsilon) \cdot \lambda_s \tag{5}$$

where $\varepsilon$ is the porosity of the material, and the subscripts $f$ and $s$ are referred to the fluid (air) and solid phase respectively.

In order to apply Equation (5), the medium porosity has to be measured, as well as the thermal conductivity of the solid matrix only, keeping in mind that it is composed by cement and gravel. $\lambda_s$ was measured directly using the Transient Plane Source (TPS) method [12], which is able to provide in a single measure the thermal conductivity and the thermal diffusivity of the investigated sample. Since the aim of this work is to experimentally assess the validity of the mathematical model for dynamic insulation walls in steady-state conditions, only the first parameter will be reported in this paper. For this purpose, we produced 8 samples with the same mix-design described in Table 1, but using fine aggregates (sand and gravel with a diameter of 1-2 mm) only. In this way we were able to obtain very compact samples (porosity around 0%) with the same over-all properties of the solid matrix of the wall sample shown in Figure 1. After a series of TPS measurements the thermal conductivity was found to be $\lambda_s$ = (1.76 ± 0.08) W/(m·K). In order to obtain the porosity $\varepsilon$, the Archimedes method was used, as suggested in [10], obtaining $\varepsilon$ = (30 ± 2) %.

At this point, assuming an air thermal conductivity $\lambda_f = 0.025$ W/(m·K), which corresponds to a temperature of 15°C, and using Equation (5), the thermal conductivity of the porous material was evaluated as $\lambda_w = (1.24 \pm 0.09)$ W/(m·K).

Moreover, by means of image analysis we were able to assess the granulometry distribution of pores inside no-fines concrete (Fig. 2), which is mainly distributed in the range 0-8 mm, with only few detections with bigger diameters (maximum at 12.5 mm). The characterization of the microscopic structure of no-fines concrete will be discussed in detail in a future publication.

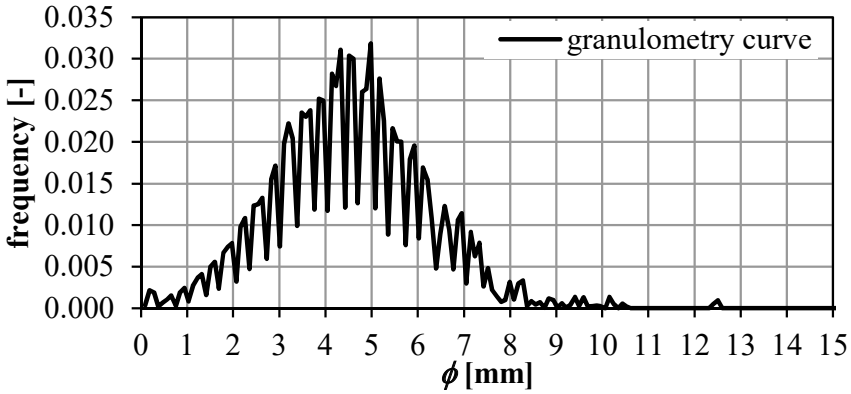


Fig. 2. Granulometry distribution of pores size inside no-fines concrete.

### *3.2. The Dual Air Vented Thermal Box*

In the last few years, an experimental apparatus was built in the Building Physics Laboratory of the Energy Department of Politecnico di Milano, allowing to test medium size samples of building envelope technologies (such as dynamic insulation).

The facility was designed in order to reproduce operative temperature boundary conditions across the sample envelope component, either in steady or unsteady state. If the sample wall is made of permeable materials, the facility can force an airflow through it, with a velocity flow rate controllable both in terms of verse and magnitude. Therefore, due to these peculiar features, no guidelines from literature could be used in the design phase: the only technical standard available [13] deals with Guarded (GHB) and Calibrated (CHB) Hot Box facilities, both aimed at the characterization of steady-state properties of non-pervious building envelope components. Even when dynamic insulation walls were investigated [5], a basic set-up was used, allowing only a partial control of thermal boundary conditions.

The design process led then to the construction of the Dual Air Vented Thermal Box shown in (Fig. 3). The DAVTB facility is mainly composed by two insulated chambers (“Boxes”) divided by the sample, a hydraulic loop and an airflow loop.

The hydraulic loop is made of a primary loop connected to a hot and a cold water tank, and a secondary loop divided into three branches, that circulate water into the radiant finned stripes in each Box (Fig. 4) and into the water-to-air heating/cooling coil. This way the operative temperature in each chamber and the airflow inlet temperature can be controlled separately.

A detailed description of the geometrical and technological characteristics, and a preliminary characterization of the hydraulic loop can be found in [8], while the control strategy and the airflow loop operation have been recently improved and will be described here.

Fig. 3. Picture of the DAVTB facility. The boxes (with the interposed sample frame) are visible, together with the hydronic plant and the air recirculation system.

Fig. 4. Internal view of one of the chambers. Radiant panels and thermocouples are visible.

The airflow loop is composed by three sections: the heating/cooling coil, the fans (two centrifugal facing in opposite direction, and four butterfly shutters) and the measurement section (a 2 m long tube – inner diameter 50 mm – with a small two-directional fan anemometer located in the middle). The airflow rate across the sample can be varied in the range 0 - 0.013 $m^3/(m^2 \cdot s)$, that is typical for Breathing Walls operation.

All the measurement and control activities are automatically performed by a multifunctional switch unit remotely controlled by a LabVIEW algorithm. The multifunctional switch is an Agilent 34980A, equipped with modules suitable for three main purposes: the first is used for voltage and current measurement (34921A/T); the second is a proportional controller and waveform generator (34951A/T); the third and last one is an ON/OFF controller (34938A/T). All electrical devices in the facility (water pumps, hydraulic valves and air shutters) are activated using the ON/OFF switches, while the proportional modules are used to regulate mixing valves and diverter to achieve the

desired supply temperature to the terminals in the hydraulic plant, to partially open or close the proportional shutters in the ventilation plant and, finally, to produce the waveform needed to affect the rotational velocity of fans through the PWM controller.

As far as data collection is concerned, the apparatus is equipped with a differential micro-manometer, a bidirectional fan anemometer (already mentioned above), a series of thermocouples for air, sample and water temperature measurement, two globe thermometers and two heat flux sensors.

All thermal probes in the DAVTB facility are T-type thermocouples (copper-constantan). In the hydronic plant needle thermocouples are used to measure water temperature in two points of each tank, and in the main points of the plant itself: hot and cold side before the mixing valves; supply to and return from the delivery systems inside the apparatus. Air temperature is measured in nine points inside each chamber, disposed in the edges and in the centre of a cubic arrangement, allowing to detect any thermal stratification phenomena. It is important to mention that every thermocouple has been shielded from the radiative heat exchange by custom made copper cylinders. Moreover, in each chamber a globe thermometer has been installed in the geometrical centre to measure the operative temperature. Some of the mentioned sensors are visible in **Errore. L'origine riferimento non è stata trovata.** Finally, it is possible to measure temperature inside the samples mounted in between the chambers. As stated before, for the purpose of this work, data have been collected from 11 thermocouples positioned along the cross section in the middle of the investigated sample.

The implemented control strategy is based on a mixed Proportional and ON/OFF approach. Operative temperatures in the Boxes and airflow inlet temperature in the upstream Box are the process variables for the ON/OFF controller, that acts on the circulators switching. The supply water temperatures in the three distribution branches are the process variables for the P controller (optimized by means of the Ziegler-Nichols method), that acts on the electric mixing valves. The stability of the control system and strategy will be demonstrated in the next section.

## 4. Results and discussion

The sample Breathing Wall described in Section 3 was tested in contra-flux configuration at four different air velocities. Firstly, the null velocity case, in which the Breathing Wall acts as a traditional wall, was tested and used as the reference condition. Then the average air velocity across the sample was imposed equal to 0.003 m/s, 0.006 m/s and 0.012 m/s. As far as boundary conditions are concerned, operative temperatures in the two chambers were set at 15°C and 40°C, obtaining an overall temperature difference of 25°C, which is suitable to represent winter conditions. It is important to notice that temperature difference is the relevant parameter, while absolute temperatures are less important since the variation of the thermal conductivity with temperature can be considered a second order effect. All the tests lasted at least two days, in order to guarantee steady state conditions.

The effectiveness of the control strategy previously described can be inferred from As stated above, during each test the temperature distribution along the cross section in the middle of the sample was measured. Going into more detail, data were collected every 5 s, and then time-averaged since steady state is reached. Results are then compared with the analytical curves coming from the physical model described by Equation (4). Clearly in the first test, where no airflow is crossing the sample, a linear temperature distribution was expected.

Table 2. In the table the time-average velocity $<u>$ derived from measurements is compared with the desired value $u_{sp}$ for each test performed. Since the anemometer ac-curacy after calibration has been assessed as $1.26 \cdot 10^{-4}$ m/s, the discrepancies between set-point and measured values can be neglected. At the same time, temperature control algorithm proves to be effective in both chambers: the difference between the desired values (15°C in Box 1 and 40°C in Box 2) and the corresponding measurements aver-age is always below 0.1°C. Moreover, both operative temperatures seem to be stable in time, given that their deviations from the set-point are generally within the range ±0.2°C. Even though the temperature differences between chambers show grater deviations from the expected value of 25°C, their value is always lower than 0.5°C in module. Due to all these observations, the thermal conditions achieved can be considered representative of steady-state phenomena, and consistent in all tests.

As stated above, during each test the temperature distribution along the cross section in the middle of the sample was measured. Going into more detail, data were collected every 5 s, and then time-averaged since steady state is

reached. Results are then compared with the analytical curves coming from the physical model described by Equation (4). Clearly in the first test, where no airflow is crossing the sample, a linear temperature distribution was expected.

Table 2. Average values of the boundary conditions achieved during the four tests.

| | | BOX 1 | | | | |
|---|---|---|---|---|---|---|
| | airflow | | | error | | |
| ID | <u> [m/s] | <$T_1$> [°C] | std.dev. [°C] | mean [°C] | min [°C] | max [°C] |
| 1 | 0 | 15.03 | 0.05 | -0.03 | -0.17 | 0.12 |
| 2 | 0.00296 | 15.02 | 0.04 | -0.02 | -0.14 | 0.12 |
| 3 | 0.00604 | 14.96 | 0.07 | 0.04 | -0.11 | 0.23 |
| 4 | 0.01201 | 14.99 | 0.05 | 0.02 | -0.11 | 0.18 |

| | | BOX 2 | | | | |
|---|---|---|---|---|---|---|
| | airflow | | | error | | |
| ID | <u> [m/s] | <$T_2$> [°C] | std.dev. [°C] | mean [°C] | min [°C] | max [°C] |
| 1 | 0 | 39.96 | 0.04 | 0.04 | -0.09 | 0.20 |
| 2 | 0.00296 | 39.94 | 0.03 | 0.06 | -0.05 | 0.22 |
| 3 | 0.00604 | 39.95 | 0.04 | 0.05 | -0.05 | 0.22 |
| 4 | 0.01201 | 39.93 | 0.05 | 0.08 | -0.06 | 0.35 |

| | | TEMPERATURE DIFFERENCE | | | | |
|---|---|---|---|---|---|---|
| | airflow | | | error | | |
| ID | <u> [m/s] | <ΔT> [°C] | std.dev. [°C] | mean [°C] | min [°C] | max [°C] |
| 1 | 0 | -24.94 | 0.06 | -0.06 | -0.31 | 0.11 |
| 2 | 0.00296 | -24.92 | 0.05 | -0.08 | -0.27 | 0.09 |
| 3 | 0.00604 | -24.99 | 0.08 | -0.01 | -0.27 | 0.21 |
| 4 | 0.01201 | -24.94 | 0.07 | -0.06 | -0.42 | 0.15 |

For the tests from 2 to 4 (please refer to As stated above, during each test the temperature distribution along the cross section in the middle of the sample was measured. Going into more detail, data were collected every 5 s, and then time-averaged since steady state is reached. Results are then compared with the analytical curves coming from the physical model described by Equation (4). Clearly in the first test, where no airflow is crossing the sample, a linear temperature distribution was expected.

Table 2 for the IDs), the value of the respective A parameter was calculated according to Equation (3), considering the time-average measured velocity <$u$> from As stated above, during each test the temperature distribution along the cross section in the middle of the sample was measured. Going into more detail, data were collected every 5 s, and then time-averaged since steady state is reached. Results are then compared with the analytical curves coming from the physical model described by Equation (4). Clearly in the first test, where no airflow is crossing the sample, a linear temperature distribution was expected.

Table 2, the sample thermal conductivity $\lambda_w$ derived from measurements, and assuming thermo-physical properties of air at 15°C, corresponding to the condition of air entering the sample. Indeed, it was proved that computing air

properties at 40°C, which is the upper limit for the air leaving the sample, leads to negligible alterations on the temperature distribution (the difference is below 0.13°C in the worst case).

In Fig. 5 measured temperature profile data are compared to the corresponding analytical curves obtained with $A = A_{calc}$. First, it can be remarked that, as the air velocity increases, deviation from the linear trend increases. Secondly, it is possible to observe that the experimental data are well represented by the physical model described in literature: the mean standard deviation between the analytical model profile and the measured profile is equal to 0.15 °C, 0.11 °C and 0.12 °C for test 2, 3 and 4 respectively. Moreover, the agreement between the experimental outcomes and the model provides a confirmation of the measured thermal conductivity value for the no-fines concrete solid matrix, reported in Section 3.1.

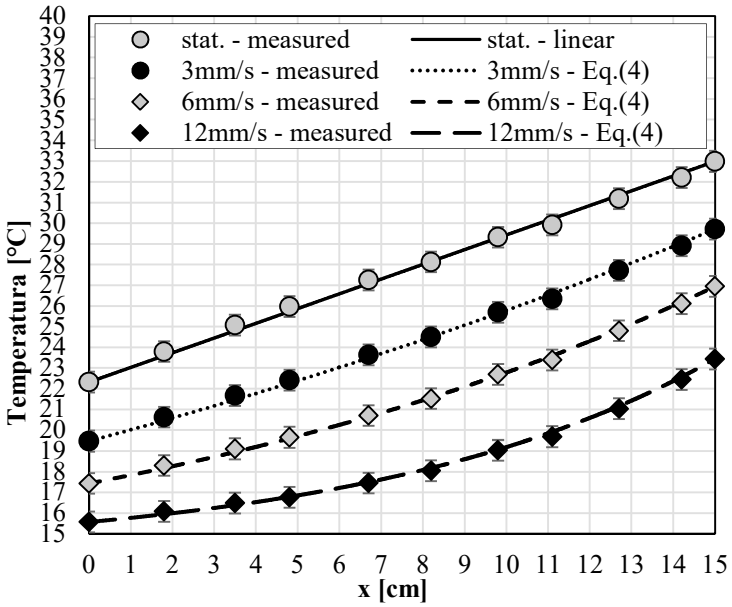


Fig. 5. Temperature distribution inside the sample (centre section) at different air velocities: measured data and analytical model curves based on $A_{calc}$.

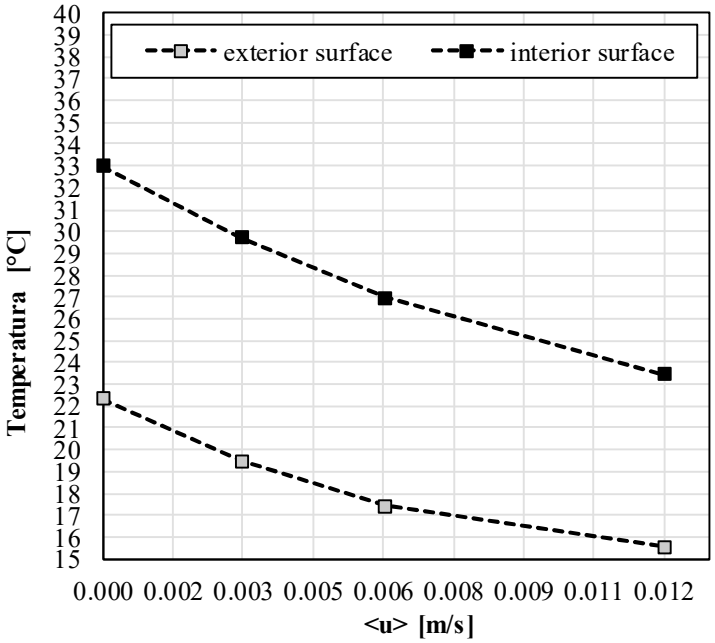


Fig. 6. Interior (towards Box 2) and exterior (towards Box 1) surface temperature as a function of average velocity of the air crossing the sample.

In Fig. 6 the effects of the velocity of the airflow on the surface temperatures are shown. In fact, many previous works [5],[14],[15] state that one of the effects of contra-flux regime is the surface temperature drop on both sides of the Breathing Wall, which is clearly highlighted by the outcomes from the laboratory tests reported here. Further it can be noticed that, at the highest velocity adopted namely 0.012 m/s the wall exterior surface temperature, namely facing the cold chamber, almost reached the asymptotic value of 15°C equal to the operative temperature in Box 1.

At the same time, the temperature distribution calculated for each test in Breathing Wall working condition was processed into the Matlab Curve Fitting Toolbox, deriving the A parameter through fitting of Equation (4). In Table 3 $A$ from fitting ($A_{fit}$) is compared with $A$ from calculation ($A_{calc}$). It can be remarked that, considering the errors, the two parameters agree with each other.

Table 3. Comparison between $A$ parameter from calculation ($A_{calc}$) and from fitting ($A_{fit}$).

| ID | $A_{calc}$ [$m^{-1}$] | $A_{fit}$ [$m^{-1}$] |
|---|---|---|
| 1 | - | - |
| 2 | 2.95 (±0.34) | 2.51 (±0.78) |
| 3 | 6.03 (±0.57) | 5.94 (±0.60) |
| 4 | 11.98 (±1.01) | 12.40 (±0.83) |

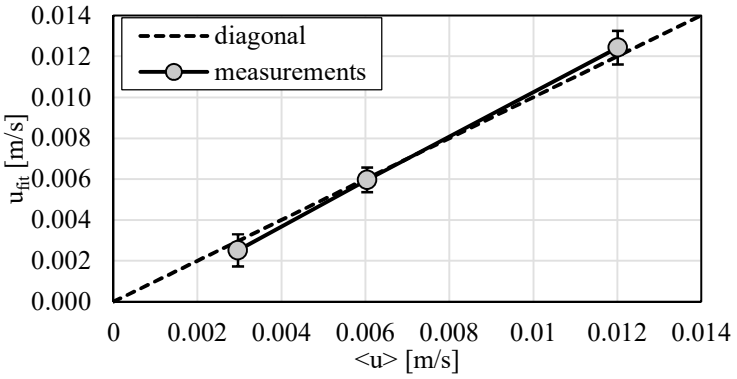


Fig. 7. Average air velocity derived from fitting $u_{fit}$ versus measured average air velocity crossing the sample <u>.

Finally, the values of $A_{fit}$ reported in Table 3 have been used to derive comparative values of airflow velocity ($u_{fit}$) by reversing Equation (3). Results of this calculation are compared to the measured average velocity in Fig. 7. Since the effective velocity profile of the airflow, approaching the sample, is not directly measured in the DAVTB apparatus, this way we have been able to assess that the desired average velocity is actually achieved in the middle of the Breathing Wall.

## 5. Conclusions

By means of the DAVTB apparatus, for the first time to the best of the authors' knowledge the steady state temperature profile in a Breathing Wall was measured at variable airflow velocity crossing the wall. The measured data exhibit the characteristic exponential trend predicted by the analytical model by Taylor and Imbabi. In order to assess the validity of the model, the no-fines concrete thermal conductivity was obtained. Indeed, a very good agreement is observed between experimental temperature profiles in the middle of the sample wall and the model predictions.

Further investigations will consider verifying the temperature profile in different portions of the sample, connected to the uniformity of the air velocity profile on the wall surface, and studying multilayers Breathing Walls. Moreover, since the DAVTB apparatus allows establishing variable operative temperatures, the Breathing Wall behavior in transient state will be investigated.

The present study is carried out within the Cost Action TU 1403 Adaptive Façade Network.

## References

[1] Brunsell J.T. The performance of Dynamic Insulation in two residential buildings. Air Infiltration Review 1995;16:7-11.
[2] Taylor B.J., Imbabi M.S. The application of dynamic insulation in buildings. Renewable Energy 1998;15:377-382.
[3] Craig S., Grinham J. Breathing walls: The design of porous materials for heat exchange and decentralized ventilation. Energy and Buildings 2017;149:246-259.
[4] Taylor B.J., Cawthorne D.A., Imbabi M.S. Analytical investigation of the steady-state behaviour of dynamic and diffusive building envelopes. Building and Environment 1996;31:519-525.
[5] Taylor B.J., Imbabi M.S. The effect of air film thermal resistance on the behaviour of dynamic insulation. Building and Environment 1997;32:397-404.
[6] Dimoudi A., Androutsopoulos A., Lykoudis S. Experimental work on a linked, dynamic and ventilated wall component. Energy and Buildings 2004;36:443-453.
[7] Di Giuseppe E., D'Orazio M., Di Perna C. Thermal and filtration performance assessment of a dynamic insulation system. Energy Procedia 2015;78:513-518.
[8] Alongi A., Mazzarella L. The Dual Air Vented Thermal Box: a laboratory apparatus to test air permeable building envelope technologies. Energy Procedia 2015;78:1543-1548.
[9] Nield D.A., Bejan A. Convection in Porous Media – Third Edition. USA: published by Springer. 2006.

[10] Wong J.M., Glasser F.P., Imbabi M.S. Evaluation of thermal conductivity in air permeable concrete for dynamic breathing wall construction. Cement & Concrete Composites 2007;29:647-655.
[11] Kaviany M. Principles of Heat Transfer in Porous Media – second Edition. New York: published by Springer. 1995.
[12] He Y. Rapid thermal conductivity measurement with a hot disk sensor – part 1. theoretical considerations. Thermochimica Acta 2005;436:122-129.
[13] ISO. Thermal insulation. Determination of steady-state thermal transmission properties. Calibrated and guarded hot box. ISO 8990 Standard. Geneva: International Organization for Standardization. 1994.
[14] Krarti M. Effect of air flow on heat transfer in walls. Journal of Solar Energy Engineering 1994;116:35-42.
[15] Gan G. Numerical evaluation of thermal comfort in rooms with dynamic insulation. Building and Environment 2000;35:445-453.